Rock Mech. Rock Engng. (1999) 32 (2), 101–122

Rock Mechanics and Rock Engineering

Deformation Mechanism of the Underground Excavations at the WIPP Site

By

S. Kwon and **J. W. Wilson**

Department of Mining Engineering, University of Missouri, Rolla, U.S.A

Summary

The deformational behavior of underground excavations in rock salt is difficult to predict because of the time-dependent properties of rock salt, and its response to many other parameters, which influence its behavior. To investigate the influence of important parameters such as time, temperature, geology, opening geometry, excavation sequence, and effects of the immediate roof layer on underground excavations in rock salt, deformation measurements from the Waste Isolation Pilot Plant (WIPP) were used.

1. Introduction

Natural salt deposits are considered desirable host rocks for permanent disposal of nuclear waste material because of unique properties such as low permeability, high heat conductivity, and ductility. At room temperature and pressure, such rock salts are the most ductile of all the rock types (Baar, 1977). Because of this ductility, underground excavations in rock salt show significant time-dependent deformational behavior. Due to the time-dependent properties of rock salt, as well as its response to many other parameters which influence its behavior, the deformational behavior of the underground openings in rock salt is complex.

The time-dependent deformation of rock salt, which is usually called creep, consists of four stages, namely: an elastic deformation stage, a transient or primary creep stage, a steady state or secondary creep stage, and a tertiary creep stage. The instantaneous elastic deformation occurs immediately after the creation of an excavation and is followed by the primary creep stage. In this primary creep stage, a high deformation rate decreases exponentially with time. The exponential decrease of the deformation rate under constant load in laboratory creep tests can be described as a strain hardening effect. The strain hardening effects can occur by dislocation pile-ups at numerous obstacles such as grain boundaries and impurities (Senseny et al., 1992). The decay of the deformation rate of an excavation, how-

ever, is not due to the strain hardening effect, but mainly due to stress-relief (Baar, 1977). The stress relief creep due to stress reduction is a major reason for the differences between the predictions based on laboratory tests and in situ observations (Baar, 1974). The secondary creep stage, which follows the primary creep stage, is characterized by a constant or near constant creep rate over a relatively long period of time. Reaching the secondary creep stage in the lab requires several weeks (Hambley et al., 1988). During the tertiary creep stage, the strain rapidly accelerates toward rupture of the rock salt.

Computer simulations are currently the most popular method to describe the deformational behavior of a rock mass around an excavation. Even though these techniques have many advantages, there are clear limitations to their use. Firstly, if the in situ physical and mechanical properties of the rock are not precisely known, computer simulations cannot produce reliable results (Sakurai, 1991, 1993). For example, the separation at a clay seam above the mining horizon is an important factor in determining the stability of openings, but the properties of the clay seam which determine the separation process are not yet precisely known. Secondly, changes in the mechanical and physical properties of the rocks after excavation are sufficiently significant that the values obtained from laboratory tests and used in the model cannot accurately predict the actual deformational behavior. Furthermore, the constitutive equations required to describe these property changes, which are dependent on time and distance from the opening, are extremely complex. Because of the inherent limitations in computer simulation for predicting the deformational behavior of underground excavations in rock salt, Kwon and Miller (1995) tried to describe the actual deformational behavior of a room at the Waste Isolation Pilot Plant (WIPP), using in situ deformation measurements that included extension, closure, and deflection.

The researchers suggest that if the deformations around underground excavations are carefully measured in situ, the field measurements provide a better understanding of the deformational behavior of underground excavations. Such measurements must reflect all of the governing factors, including opening geometry, in situ stress, temperature, rock properties, geology, and excavation sequence, and the careful analysis of field measurements will identify the influence of each parameter on the deformational behavior of the opening.

2. The WIPP Facility

The WIPP is a research and development facility authorized to demonstrate the safe disposal of radioactive waste resulting from the defense projects of the United States. In 1981 the WIPP project began the construction of a facility in Carlsbad, New Mexico under the direction of the U.S. Department of Energy (DOE). The underground facility at the WIPP is located 650 m below the surface in bedded salt of the Permian Salado Formation and this facility is planned to ultimately become a repository for Transuranic (TRU) waste material. The underground facility has been divided into three areas: (1) the Site and Preliminary Design Validation (SPDV) area; (2) the Experimental area; and (3) the waste storage area. Excava-

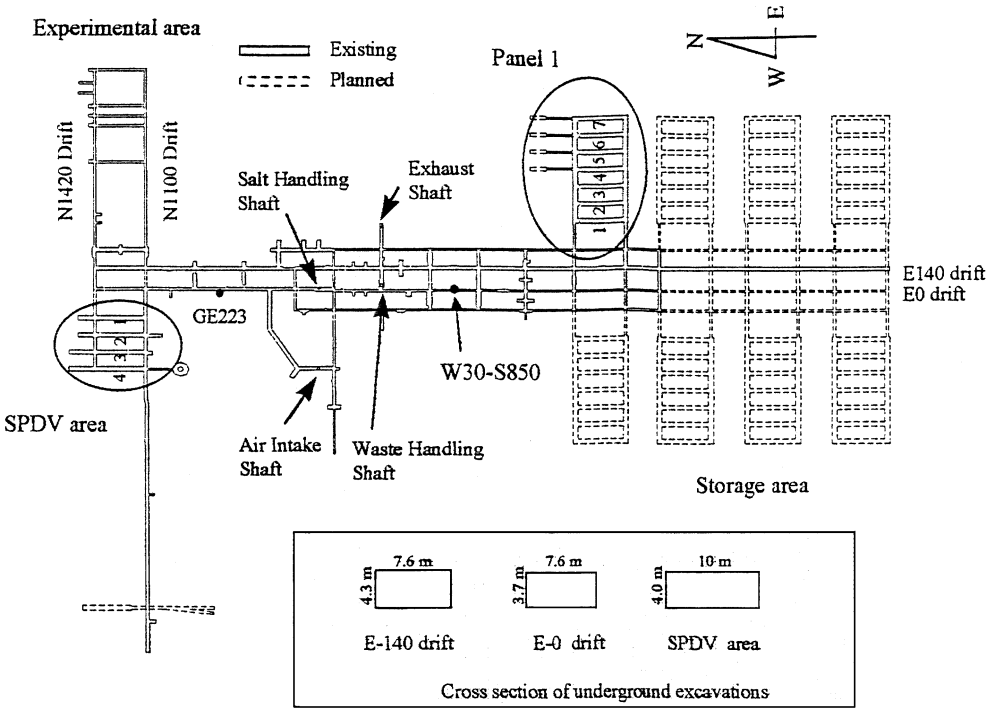

Fig. 1. Underground layout of the WIPP facility

tions of the SPDV area, the experimental area, and one panel in the waste storage area have been completed. Figure 1 shows the schematic layout of underground facilities and cross sections of drifts and SPDV rooms at the WIPP site. The storage area will ultimately be made up of eight panels consisting of seven rooms where each room is approximately 4 m high, 10 wide and 100 m long. The dimensions of the storage rooms were determined by calculations based on laboratory derived average creep parameters to satisfy the design criteria, using a vertical closure of 30 cm and a horizontal closure of 23 cm, after 5 years. The four rooms in the SPDV area have similar configurations to the rooms in the waste storage area. Among the four rooms in the SPDV area, SPDV Room 1 and Room 2 collapsed in 1991 and 1994, respectively. The configuration of the drifts range from 2.4 m to 4.3 m high and 3.7 m to 7.6 m wide. After construction, several instruments for measuring deformation of the excavations, including extensometers, closure meters, and inclinometers were installed systematically. In most cases, the first reading date was close to the excavation data and the rapid deformation immediately after the excavation was probably recorded.

The facility is sited within an evaporate sequence consisting of halite, argillaceous halite, and polyhalite. Figure 2 shows the stratigraphy in the WIPP site. Anhydrite 'b', 6.4 cm thick, lies about 2 m above the roof and is underlaid by Clay 'G'. Anhydrite 'a', about 20 cm thick, is about 4 m above the roof and underlaid by Clay 'H'. A persistent 0.5 to 0.8 m thick bed of anhydrite and polyhalite,

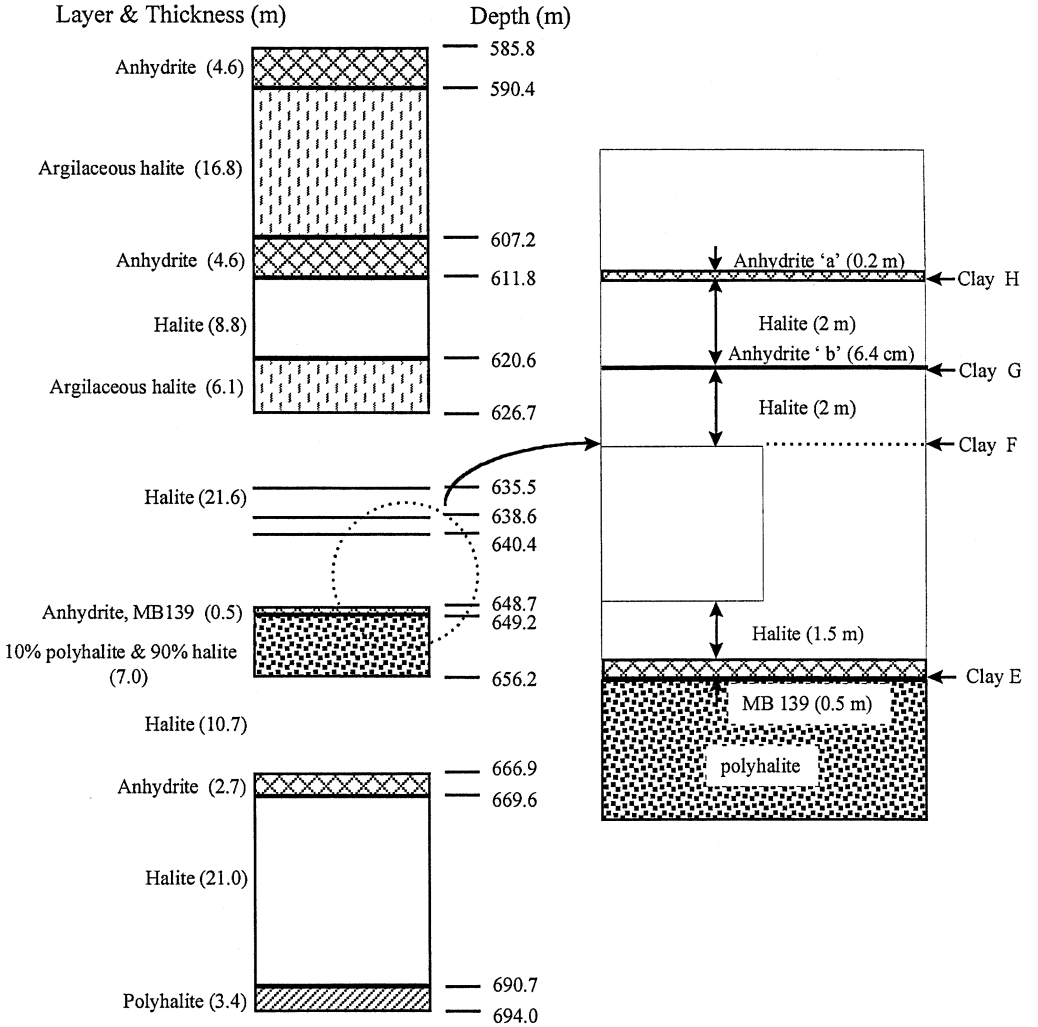

Fig. 2. Geological section at the WIPP site

identified as MB 139, lies about 1.5 m below the opening floor. Compared to the surrounding halite, MB 139 is a stiff and brittle layer that does not deform plastically with time (U.S.DOE, 1993). The bottom of MB 139 is subhorizontal and underlaid by Clay 'E'. A diffused clay, Clay 'F', is exposed in the ribs of pillars just below the roof.

3. Data Reduction

Data reduction of in situ measurements is critical for the deviation of deformation characteristics related to the governing parameters because the basic measured

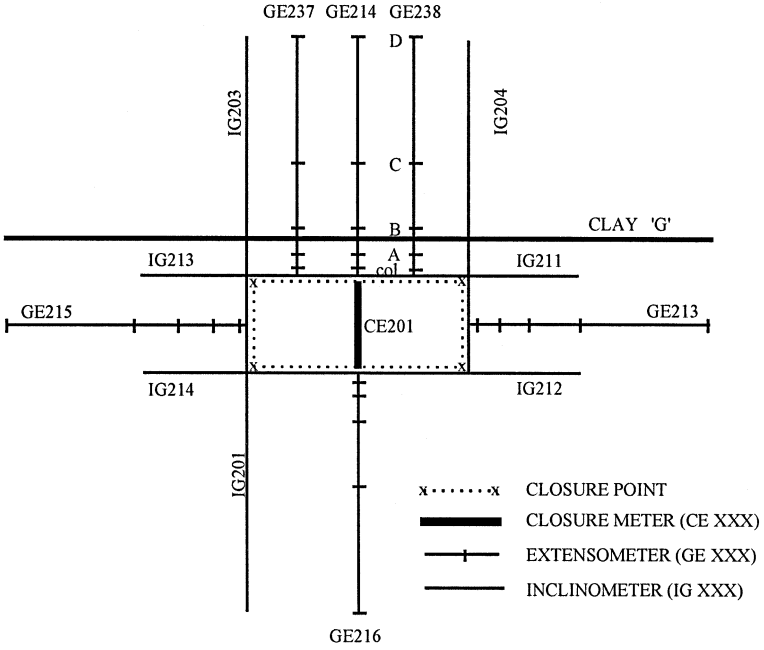

Fig. 3. Instrumentation in SPDV Room 2

data usually cannot be used directly. Possible identifiable errors in the data should be corrected before data analysis, and then the data should be plotted to allow a better interpretation of the deformational behavior around the excavation.

3.1 Data Collection

Various systems of measurement were used to monitor the performance of the underground excavations. Among them, the measurement of closure, which represented cumulative reduction of opening dimensions, was the method most generally applied. Vertical and horizontal closures were measured using a tape extensometer, which measured the distance change between reference points. Multi-position borehole extensometers (MPBX), which measured the relative displacements between the multiple anchors located at various depths in a hole, were used to obtain detailed information on deformational behavior within the rock. At WIPP, most of the extensometers had the deepest anchor placed 15 m from the opening, and up to 5 anchor stations were installed in one borehole. For remote readout, the probe was left locked to the anchor and a cable was strung to the readout station, which was connected to a remote data logger. In order to protect the probe heads, the surface anchor was recessed roughly 0.3 m inside the borehole. Another important instrument used was the inclinometer. The inclinometer provided information on rock displacements in a direction perpendicular to the

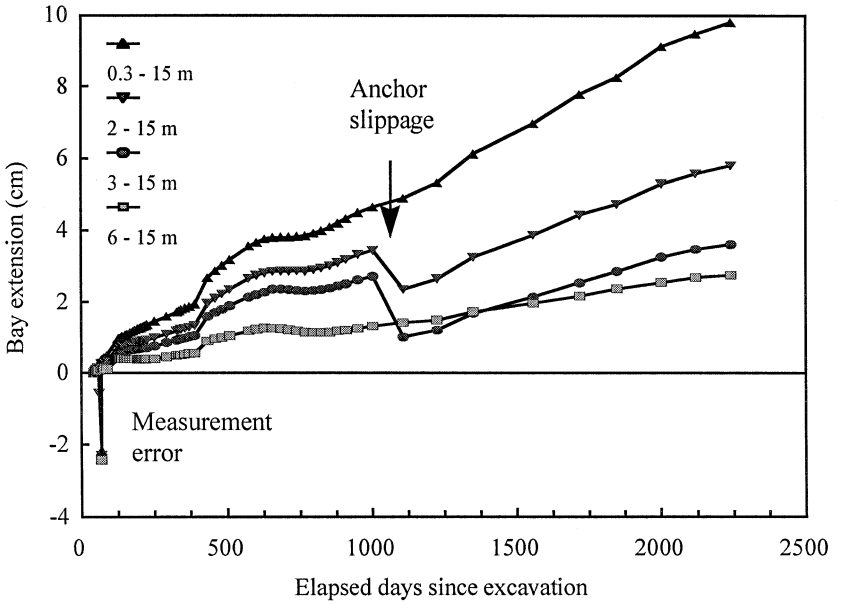

Fig. 4. Measured bay extension from an extensometer before error correction

longitudinal axis of the borehole. In the SPDV Rooms, inclinometer measurements were taken in vertical boreholes up to 15 m deep into the roof and floor. Figure 3 shows the instrumentation in SPDV Room 2.

3.2 Data Correction

Field measurements often contain erroneous data for the following reasons: (a) power failure, gage management (replacement), or disconnection of the gage; (b) low resistance shorts to ground because of the collection of moisture; (c) undetected reading error; and (d) computer acquisition error, or electrical scatter (Munson et al., 1990). Furthermore, measurements may not represent the actual deformational behavior of the opening for other reasons, such as anchor slippage or large relative horizontal movements of the layers in the roof or floor. Figure 4 shows an example of the original measurements which contained errors that arose from random error and anchor slippage.

The resolution of the extensometers used at the WIPP site is about ± 0.0025 cm. The shorter the measuring time interval, the higher is the ratio of the error of the instrument to the deformation during the measuring time interval. When the measuring interval was very short, say less than 1 day, the calculated deformation rate for that measurement was unreasonably high or low due to the instrument noise. This also needed to be corrected before the data was analyzed.

3.3 Data Manipulation

a. Smoothing: In many cases, deformation rates such as extension rate and closure rate can fluctuate widely, which makes it difficult to interpret the data. Smoothing was found to be the easiest way to reduce or eliminate the fluctuations and provided a better idea of the overall trend of deformation. However, it had to be kept in mind that information derived from the measurements could be lost or changed after smoothing. For example, smoothing can reduce the apparent effect of adjacent excavations on the deformation of a previously excavated opening. In this study, the measured data at WIPP were successfully smoothed, using a three-point moving average in order to reduce the fluctuation of measurements without losing valuable information.
b. Curve fitting: Curve fitting was one method of investigating the presence of associations, if appropriate data was available. The discovery of associations and the ability to express such associations in a precise mathematical form made the prediction of the unobservable value of a variable possible, based on the observed value of one or more associated or related variables. The best fit equation helped to determine how to control the values of one variable by manipulating the values of related variables.
c. Interpolation: The measuring interval as well as the instrument installation date was different for each instrument. In order to calculate deformation and deformation rate at a specific time after excavation and to compare the deformational behaviors from different measuring sites and different measuring intervals, interpolation was indispensable.

4. Influence of Important Parameters

Extension and closure measurements from the WIPP site were used for data analysis. A FORTRAN program was developed for manipulating the deformation measurements (Kwon, 1996). The FORTRAN program consists of the following steps:

a. Read input data: Possible input data are deformation information such as extension, strain, and closure. Excavation data and dates of interest need to be input for each data set. For the WIPP data, 20, 30, 60, 90, 200, 300 days after excavation were selected as the dates of interest. 20 days was selected because it was considered to be the earliest generally available date after the excavation date when most extensometers were operational. To ensure that the strain rate or closure rate had reached steady state conditions, 200 days and 300 days were selected.
b. Separate data according to the dates of adjacent excavations: Data must be divided into distinct periods based on the dates adjacent excavations were created. Independent smoothing for each period was necessary in order not to lose information about the influence of an adjacent excavation.
c. Data smoothing: Smoothing, using a moving average interval, was carried out separately for each period. It was possible to control the smoothing effect by

Table 1. Plotted graphs

1.	When the X-axis represents the cumulative days since excavation
	Extension relative to the farthest anchor from the opening
	Bay extension between the two anchors (Fig. 4)
	Bay strain between the two anchors
	Strain between the collar and the last anchor
	Extension rate
	Bay strain rate (Fig. 8, Fig. 9, Fig. 14)
	Strain acceleration (Fig. 10)
	Closure
	Closure rate (Fig. 13)
	Difference between the vertical convergence and sum of the roof and floor extension
	Difference between the horizontal convergence and sum of the rib extensions
	Difference between the closure rate and the extension rate
	Ratio of the extensions between two different measuring locations
	Ratio between the closure rate and extension rate
	Ratio of the strain rates between two different measuring locations
2.	When the X-axis represents the distance from the opening
	Bay strain (Fig. 18, Fig. 19)
	Bay strain rate
	Bay extension
	Bay extension rate
	Deflection from an inclinometer
3.	When the X-axis represents the real date
	Bay strain rate to check the influence of adjacent excavation (Fig. 17)
	Seasonal temperature variation (Fig. 7)

changing the moving average interval, depending on the purpose of the data analysis.

d. Calculate deformation rates: From the smoothed deformation, deformation rates such as extension rate, strain rate, and closure rate were calculated.
e. Interpolation: The calculated rates were interpolated for daily values. The rate for each date of interest, 20, 30, 60, 90, 200, 300 days after excavation, was checked. Also, the steady state creep rate was calculated from the linear part of the deformation curve.

The graphs listed in Table 1 could be plotted from deformation measurements after running the program. In the table, 'bay' represents the range between each anchor in the extensometer. From the data analysis using the deformation measurements from the WIPP site, the influence of parameters such as time, temperature, geology, opening geometry, and excavation sequence on the deformational behavior of underground excavations in rock salt could be determined. In this study, deformation rates such as closure rate and extension rates, were mainly used to investigate the influence of most parameters. Deformation rate was useful for comparing the deformational behavior of different excavations because it was independent of the installation date. In contrast, cumulative deformations, such as closure and extension, could not be meaningfully compared when the installation dates, after the excavation was created, varies. This is because a few days' delay in installation can result in the exclusion of significant early deformation data, since there is rapid deformation in the early stages of an opening life.

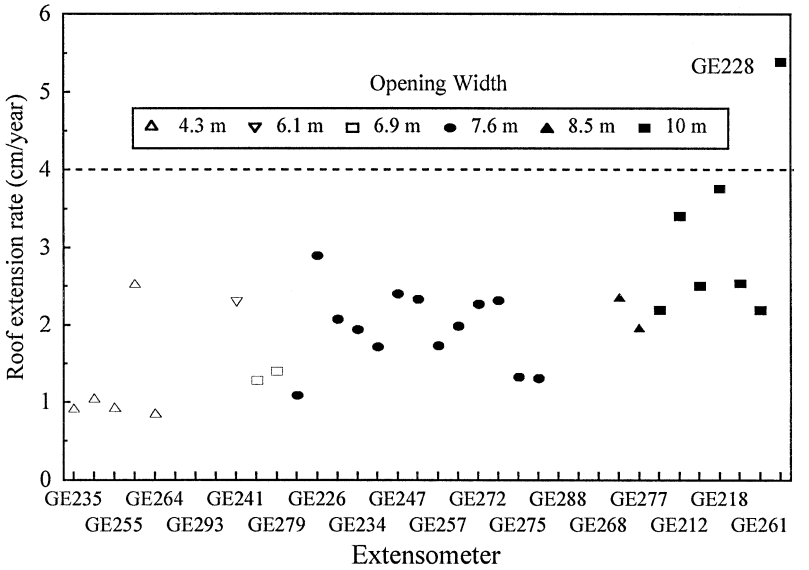

Fig. 5. Influence of opening width on the secondary creep rates

4.1. Influence of Opening Geometry

From all available roof extensometers at the WIPP site, the constant extension rates of the first 15 m in the roof in the steady state creep stage were plotted, as shown in Fig. 5. The fairly wide variation in the extension rates might be due to the influence of other controlling parameters such as opening height and pillar size. In most cases, except GE228 at the salt handling shaft, the extension rates were below 4 cm/year. This suggests that the support system for the openings in the storage area should be designed to accommodate an extension rate of 4 cm/year. From Fig. 5, the average roof extension rates were calculated and plotted in Fig. 6. The roof extension rates increased exponentially with increasing opening width. It was noted that there was a clear relationship between the opening width and extension rate, even in the secondary creep stage.

The effect of the opening geometry on the strain rate at the rib can be observed in Table 2. The average strain rates were calculated for different types of opening geometry from the extensions measured at 0.3 –1.8 m and 0.3 m–3.7 m at ribs. The three types of opening geometry referenced in Table 2, were the most important encountered at WIPP. From Table 2, it was found that the influence of the opening geometry was more significant between opening dimensions of 3.7 m × 7.6 m and 4 m × 10 m than between 2.4 m × 4.3 m and 3.7 m × 7.6 m. When the opening dimensions were changed from 3.7 m × 7.6 m to 4 m × 10 m, the strain rates in the rib increased by around 100%.

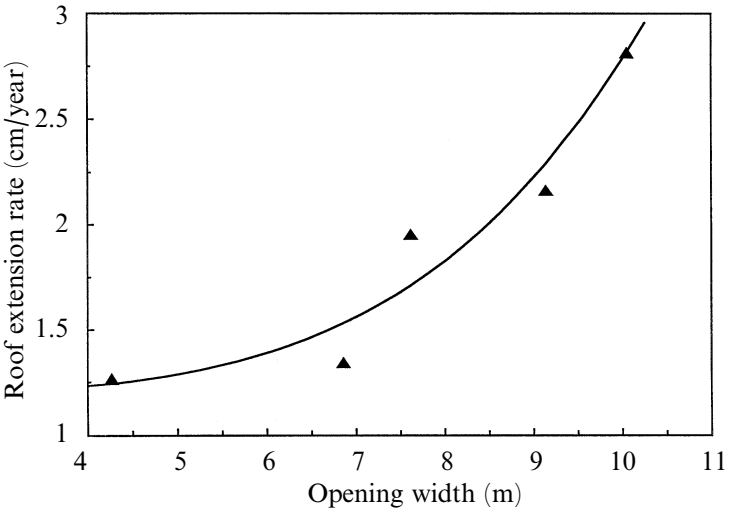

Fig. 6. Influence of opening width on the secondary roof extension rates of 0.3 m–15 m in the roof

Table 2. Average strain rate (10^{-3}/year) at ribs for different opening geometries

Measuring interval	Height × width (m) × (m)	Elapsed days since excavation 20 days	30 days	60 days	90 days	200 days
0.3 m–1.8 m	2.4 × 4.3	28	16	11	8	4
	3.7 × 7.6	32	24	11	9	7
	4.0 × 10	52	55	18	13	11
0.3 m–3.7 m	2.4 × 4.3	17	11	7	5	3
	3.7 × 4.6	21	16	7	6	5
	4.0 × 10	43	47	14	11	7

4.2 Temperature Effect

It is well known that rock salt shows highly temperature-dependent behavior. At higher temperatures, the deformation of rock salt increases due to the plastic flow promoted by the increase in ductility (Hansen et al., 1981; and Wittaker et al., 1992). The investigation of the influence of seasonal temperature changes on deformation rates is important, because this will affect the interpretation of the field data (U.S.DOE, 1989). Figure 7 shows the temperature measurements from the thermocouple borehole at the location W30-S850 (Fig. 1), which is close to the Waste Handling Shaft. The temperature variation was measured at different depths into the thermocouple borehole. The seasonal temperature variation at the opening surface, 0 m into the borehole, is about 16 °C. It decreases continuously with depth into the borehole. Because of the seasonal temperature variation, deformation measurements from the WIPP underground facility reveal seasonal fluctuations. The fluctuations are effectively obscured immediately following the excavation of openings by the high and rapidly reducing deformation rates during

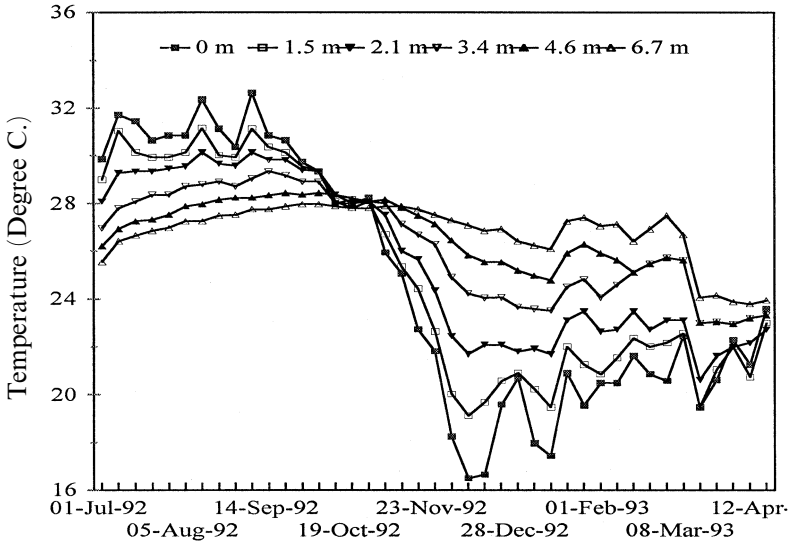

Fig. 7. Measured temperature variation at W30-S850

the primary creep stage. However, once the primary creep stage is over, seasonal fluctuations can be identified, especially at locations where the seasonal temperature variation is large (U.S.DOE, 1989). Figures 8 and 9 are the deformation rates measured from the rib extensometer, GE223 (Fig. 1), which is located at E0-N620; the deformation rates show the effect of seasonal temperature variation.

As a result of this study, the following equation is suggested in order to fit the deformation rate curves influenced by seasonal temperature variation, and then to investigated the effect of temperature on the deformation of underground excavations.

$$\dot{\varepsilon} = \left\{ A + B\cos\left(\frac{2\pi}{360}\right) \right\} \{\exp^{-Ct/365}\} + \left\{ D + E\exp\left(-\frac{t}{365}\right) \right\} \tag{1}$$

where $\dot{\varepsilon}$ is deformation rate (/year), A, B, C, D, and E are all constants without dimension and t is the elapsed days since excavation. The constants of Eq. (1) can be determined using a curve-fitting package. The first part of the above equation is necessary in order to express the periodic variation. The constant A moves the curve up or down, and B determines the amplitude of deformation rate variation due to seasonal temperature changes. The second exponential part was introduced to represent the decay of the temperature effect with elapsed time. Depending on the constant C obtained from the best fitting equation, the decay rate of the temperature effect on the deformation rate of the opening could be estimated. A higher C value indicates a more rapid decay of temperature effect with time. The last part defines the general decay pattern of the strain rate, when there is no variation related to temperature change. Figures 8 and 9 show the measured strain

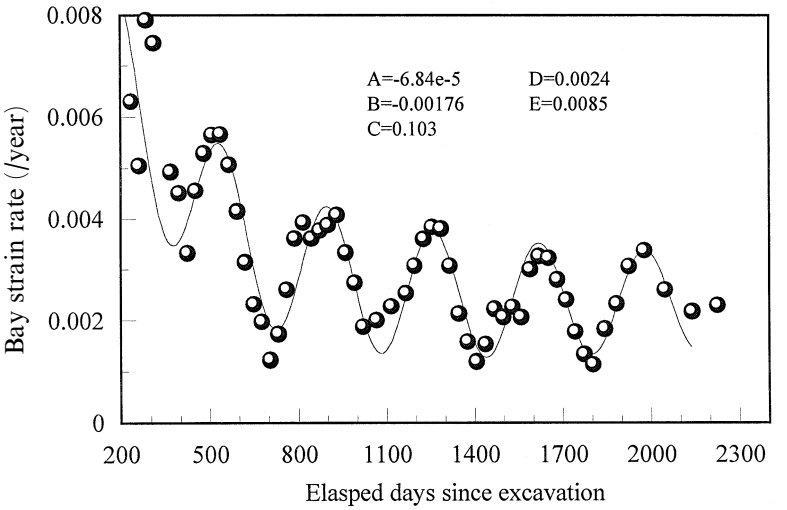

Fig. 8. Influence of seasonal temperature variation on deformation rate between 0.3 m–7.6 m of the rib extensometer, GE223

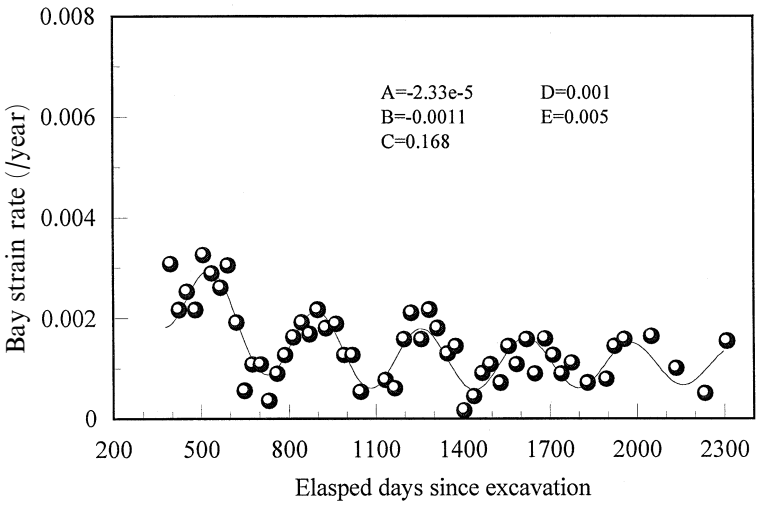

Fig. 9. Influence of seasonal temperature variation on deformation rate between 7.6 m–15 m of the rib extensometer, GE223

rates and best fit curves for the extensometer, GE223, using the above equation. By comparing the constants of the best fit curves, it was possible to estimate the effect of temperature on the deformational behavior of the underground excavation. For example, more rapid decay of the temperature effect was expected in the zone of 7.6 m–15 m than the zone of 0.3 m–15 m, because the constant C was 0.168 in the zone of 7.6 m–15 m, while it was 0.103 in the zone of 0.3–7.6 m.

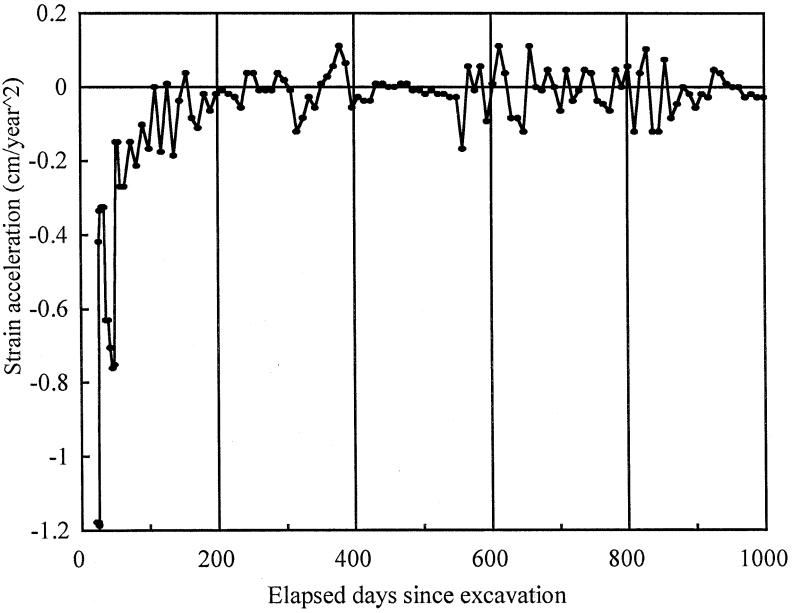

Fig. 10. Strain acceleration of the SPDV Room 1 roof

4.3 Time Effect

Determination of the transition time from the primary creep stage to the secondary creep stage is essential for defining the deformational behavior of an opening in rock salt. If the transition time is adequately known, it is possible to predict the overall deformation with reasonable accuracy by extrapolating the creep rate of the secondary creep stage, which is a constant.

The estimation of the transition time based on laboratory tests was not suitable for field conditions for several reasons. Most critically, the strain hardening effect observed in the laboratory tests does not exist in situ (Baar, 1977). Thus it is considered realistic to determine the transition time directly from field measurements. One possible way to determine the transition time from field measurements is by plotting the acceleration of the deformation. Since the acceleration will be zero in the steady state creep stage, the transition time can be easily determined from the acceleration curve. Figure 10 shows the strain acceleration of an opening at WIPP. In this case, 200 days after creating an excavation could be defined as the transition time, since the acceleration was sensibly zero after 200 days.

Another way to determine the transition time was to plot all strain rates on a single graph. A Box-Whisker plot was useful for this, since it could effectively describe the mean and distribution of several sets of data in one graph (Verdeman, 1993). In the Box-Whisker plot, the edges of the box enclose the middle 80% of the distribution, while the "whiskers" define the outlying 5% of the data values. Figure 11 illustrates a Box-Whisker plot. Figure 12 is the Box-Whisker plot of the first 15 m strain rates in the roof of the excavations at WIPP. The secondary strain

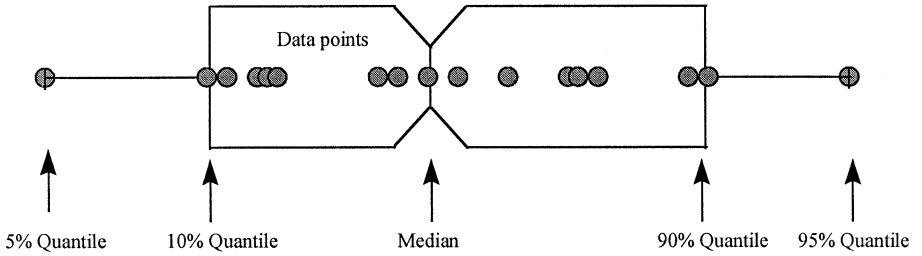

Fig. 11. The Box-Whisker plot

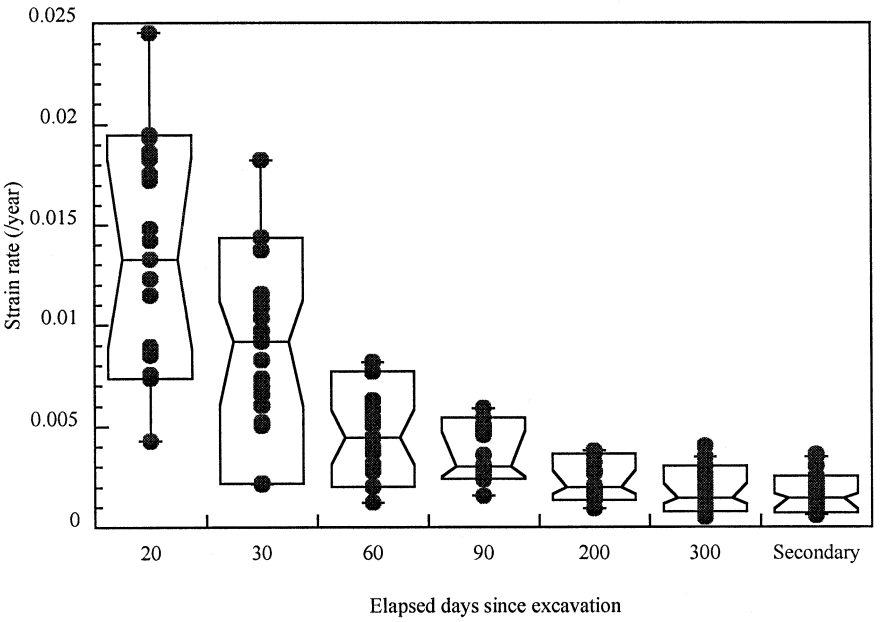

Fig. 12. Box-Whisker plot of roof strain rate (0.3 m–15 m) at WIPP

rates in the plot were calculated from the linear part of the extension curves. The distribution of the roof strain rates at 200 days after excavation was almost the same as that at 300 days, as well as during the secondary creep stage. Based on these two methods, 200 days after creating the excavation was determined as the transition time for the creep deformation at WIPP.

The secondary strain rates in the early stages were distributed over a wide range, while they converged after 200 days. This indicated that the strain rates in the early stages were influenced by other factors, which could include opening geometry, pillar size, or excavation sequence. Since the controlling factors had a more pronounced influence on the early deformation than on the deformation in the secondary creep stage, careful investigation of the primary creep deformation could lead to relationships between the deformational behavior of the underground excavations in rock salt and the controlling factors.

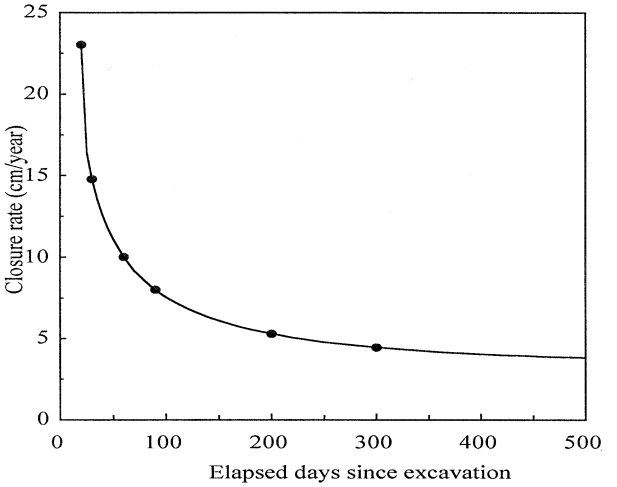

Fig. 13. Average vertical closure rates at WIPP; Dots represent the measured closure rates and curves represent the fitting curve

By plotting the average deformation rates from all measuring locations, it is possible to derive the general deformation pattern. The average closure rate was calculated from all vertical closure measurements at WIPP and plotted with time as shown in Fig. 13. Using a curve fitting package, the best fitting equation for the average vertical closure rates at WIPP was determined to be:

$$\dot{C} = -1.014 + 0.0619t^{0.5} + \frac{85.77}{t^{0.5}} + 2.35 \times 10^{9}\exp(-t) \qquad (2)$$

where, t is the elapsed days since excavation and $\dot{C}$ is the vertical closure rate (cm/year). The fitting equation in Fig. 13 shows that the vertical closure rate at WIPP decreases exponentially with time increase after excavation.

4.4 Deformation of the Immediate Roof Layer

Figure 14 shows the distribution of the roof strain rates at different times, contrasting deformations between 0.3 m and 2.4 m with those between 2.4 m and 15 m. The roof strain rates can be calculated by dividing the extension measurements from the roof extensometers by the measuring distances and the measuring time intervals. The higher strain rate in the first 2.4 m implies that the rock salt in the immediate roof layer, i.e. the layer adjacent to the roof, was more active, compared to the deeper rock layers. Two possible causes for more active deformation in the immediate roof are: (a) fracturing in the immediate roof layer due to the development of shear stress; and (b) bed separation across the clay 'G', lying at about 2 m above the roof (Fig. 2). When the immediate roof layer, deteriorated by fracturing and separation, was removed, the opening was more stable than if the layer was left.

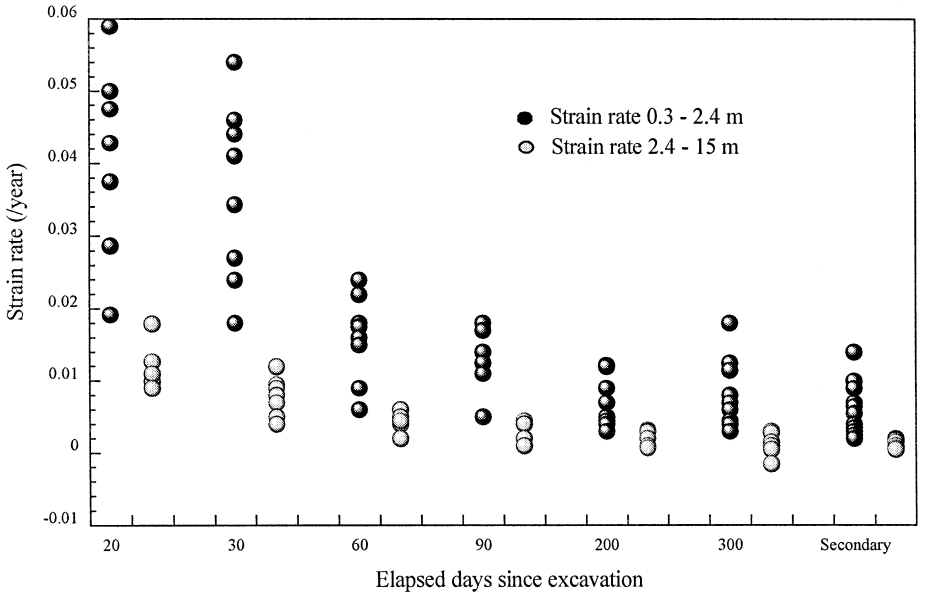

Fig. 14. Comparison of roof strain rates between 0.3 m–2.4 m and 2.4 m–15 m

The removal of the roof layer to stabilize the excavations was extensively investigated at the WIPP site from in situ observations and computer simulation (U.S.DOE, 1994). The field data indicated that removal of the highly fractured roof layer significantly improved the stability of the excavations (U.S.DOE, 1994). In the Salt Handling Shaft Station for instance, between 0.9 m and 2.4 m of salt were removed from the roof about 5.33 years after the initial excavation. Figure 15 shows the deformation rates of a roof extensometer in the Salt Handling Shaft Station. The deformation rate after the removal of the roof beam decreased from about 6 cm/year to about 1.5 cm/year as shown in Fig. 15. This indicated that the Salt Handling Shaft Station was stabilized after the removal of the roof beam.

4.5 Influence of an Adjacent Excavation

When an excavation is created near a measuring location, the deformation of the location changes due to the adjacent excavation. The characteristics of the response of the rock around an excavation to the adjacent excavation are important for choosing optimum excavation sequences. In the SPDV area, the rooms were excavated in the following sequence: Room 2 (March 10, 1983), Room 3 (March 25, 1983), Room 1 (April 4, 1983), and Room 4 (April 20, 1983). The rooms in the SPDV area are 4 m high, 10 m wide, and 100 m long and 30 m wide pillars exist between the rooms. The dimensions of the openings and pillars in the SPDV area and drifts are illustrated in Fig. 16. The extensometers installed in the roof, floor,

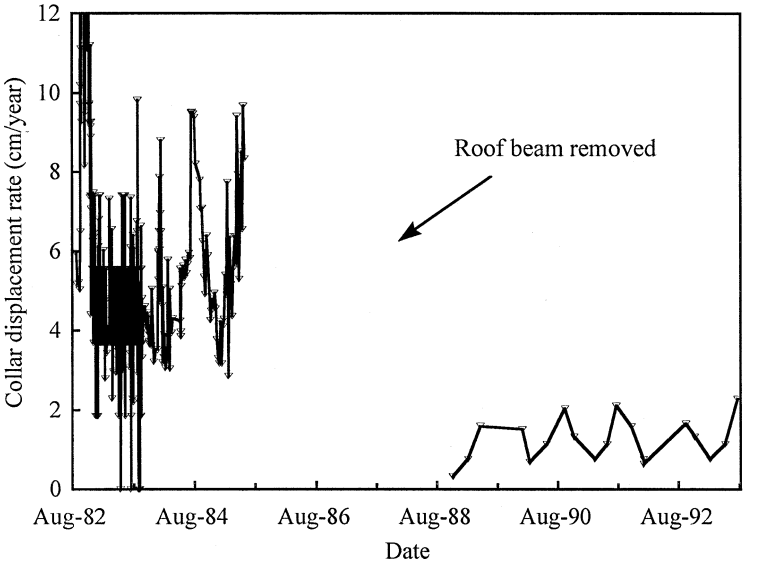

Fig. 15. Deformation rate change after the removal of the roof beam in the Salt Handling Shaft Station

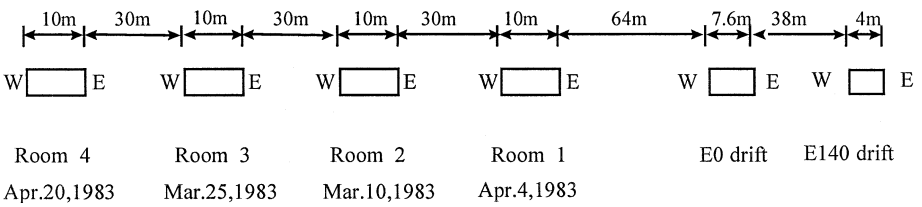

Fig. 16. Dimensions and excavation dates of the openings in the SPDV area

and ribs as well as the closure measurements, show the influence of adjacent excavations on the deformation in the pre-excavated openings.

Figure 17 shows the effect of the sequence of mining on strain in the pillar. There was a rapid drop-off in strain rate in the Room 2 East rib, which stopped when Room 3 started to be mined on March 25. However, the rate did not increase while the rate in Room 2 West rib, closer to Room 3, increased as a result of the mining of Room 3. The most dramatic change was on the rate curve of Room 2 East rib when Room 1 began to be mined on April 4. Due to the excavation of Room 1, the bay strain rate in Room 2 East rib increased from 0.03/year to 0.06/year. The increase of the strain rate reflects the stress increase around the previously excavated openings due to the adjacent excavation. As shown in Fig. 17, the effect of adjacent excavations appeared on the strain rate curves very rapidly, even though the pillar between each opening was 30 m wide. This suggests that the stress increase caused by the adjacent excavations affected the pre-excavated openings very rapidly.

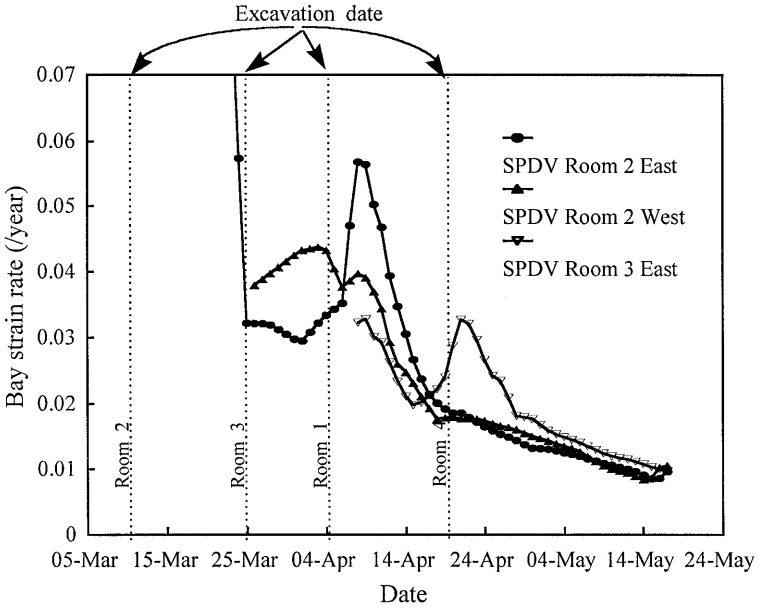

Fig. 17. Strain rate change in the ribs (0.3 m–7.6 m) due to adjacent excavations in the SPDV area

4.6 Influence of Geology

It is usually accepted that geology is one of the most important parameters which determine the overall deformational behavior of an underground excavation. If there is some difference in geology between the openings, the resultant deformation patterns in the openings could be significantly different. In other words, it would be possible to explain different deformational behaviors between the openings by investigating the difference on geology. For example, the deformation rates in SPDV Room 1 were higher than in the other SPDV Rooms (U.S.DOE, 1993). In order to understand the reason for the rapid deformation in SPDV Room 1, the geology of SPDV Room 1 and Room 2 was investigated. The geological section across the SPDV Rooms shows that the geology of the immediate roof up to Anhydrite 'b' in SPDV Room 1 is almost same as that in the other rooms. The difference in the floor geology is much more definite, as shown in Figures 18 and 19. This difference in floor geology shows up in the floor extension measurements. Figures 18 and 19 show the relationship between strain and distance into the floor. SPDV Room 2 shows a normal type of strain distribution, with a smooth change from the floor surface with depth. This indicates a zone in which the rock deforms in a continuous manner. SPDV Room 1, however, shows discontinuous strain distribution. Due to the stiff polyhalite and anhydrite layers, the deformation in the floor was initially low. The time-dependent deformation from the ductile layers below the stiff layers may have induced stress concentration in the stiff layer. This stress concentration may have caused brittle fracture of the stiff layer (U.S.DOE, 1991). The rapid increase of the strain after initially low

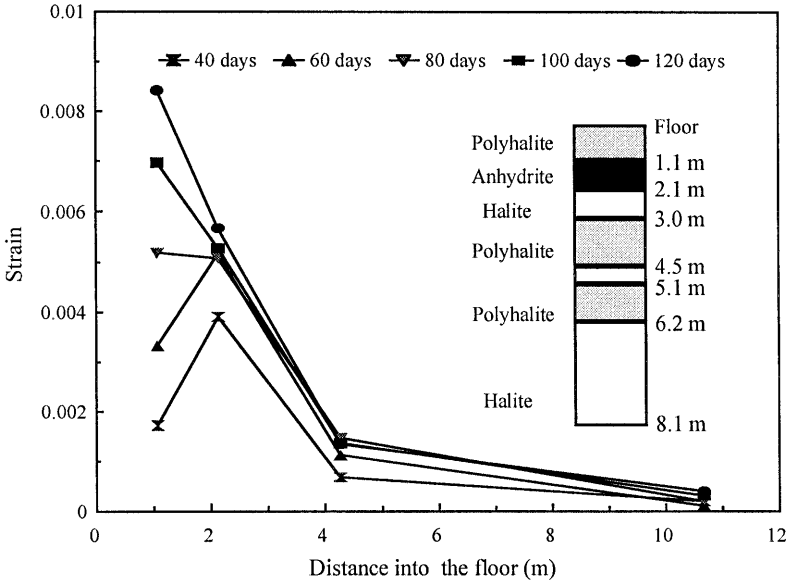

Fig. 18. Strain distribution in the SPDV Room 1 floor

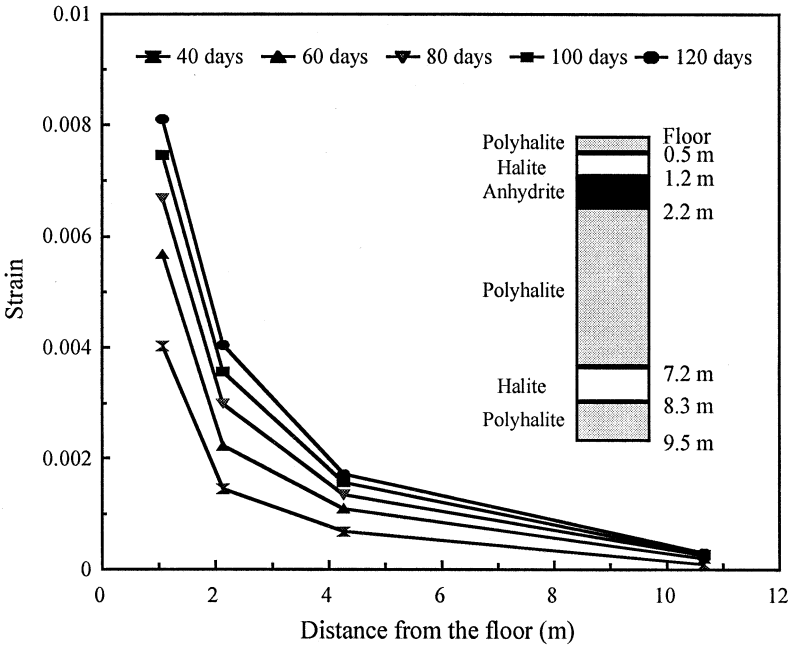

Fig. 19. Strain distribution in the SPDV Room 2 floor

strain in the SPDV Room 1 floor, reflects the fracturing in the stiff polyhalite and anhydrite layers. Thus, the discontinuous strain distribution in the SPDV Room 1 floor can be explained from the influence of the stiff anhydrite and polyhalite layers. The most significant effect of the stiffer floor on the roof behavior would be to create higher shear stresses in the roof, with an increased tendency for the pillars to punch into the roof. The end result would be faster deterioration in the roof strata.

5. Discussion and Conclusions

From the data analysis described in this paper, the following general conclusions can be drawn.

1. The transition time from the primary to the secondary creep stage can be determined from the strain acceleration plot and the Box-Whisker plot of roof strain rates. For WIPP, the transition time was about 200 days after an excavation was created.
2. There is a close relationship between the opening geometry and the deformational behavior of underground excavations in rock salt. From Table 2, it was found that the deformation rates in the primary creep stage were significantly affected by the opening geometry. For instance, the strain rates in the ribs of an opening of $4\,\text{m} \times 10\,\text{m}$ was almost 100% higher than that in $3.7\,\text{m} \times 7.6\,\text{m}$ opening. Figure 6 shows that the roof extension rates in the secondary creep stage increased more or less exponentially with increase of opening width. As shown in Fig. 5, the extension rates of the first 15 m of the roof were less than 4 cm/year, in most cases. This suggests that the support system for the openings in the storage area should be designed to accommodate an extension rate of 4 cm/year.
3. A significant influence of seasonal temperature variation on the deformation of an excavation was observed at the WIPP site. In order to fit the deformation rate curves influenced by the seasonal temperature variation, Eq. (1) was developed. By comparing the constants of the best fit curves for temperature variation, it was possible to estimate the effect of temperature on the deformational behavior.
4. The wider distribution of deformation rates in the early stages (primary creep) of excavating in rock salt (Fig. 12) indicated that the deformation of an excavation in the early stages was determined largely by controlling factors such as opening geometry, geology, temperature, excavation sequence, and the immediate roof layer. Thus, in order to determine the relationships between the deformational behavior of the underground excavations in rock salt and the controlling factors, the primary creep deformation should be carefully investigated.
5. The deformation of the roof rock adjacent to the opening is greater than that of the deeper rock layers. Removal of the roof beam stabilized the Salt Handling Shaft Station as shown in Fig. 15.
6. The deformation measurements from the ribs in the SPDV area clearly show

the influence of adjacent excavations on the deformation in the previously excavated openings. The bay strain rate in the SPDV Room 2 East rib was increased 100% from 0.03/year to 0.06/year almost immediately after the excavation of the SPDV Room 1. The rapid strain rate increase after an adjacent excavation is created suggests that the stress increase caused by the adjacent excavations very rapidly affects the previously excavated openings.

7. Geology is one of the most important parameters which determines the overall deformational behavior of an underground excavation. With careful investigation of geology, it is often possible to explain the unexpected deformational behavior of an excavation. As shown in Figs. 18 and 19, due to some difference in geology between the openings, the resultant deformation patterns in the openings was significantly different.

References

Baar, C. A. (1974): Discussion. Int. J. Rock Mech. Min. Sci. Geomech. Abstr. 11, 291–293.

Baar, C. A. (1977): Applied salt-rock mechanics. Elsevier, Amsterdam.

Hambley, D. F., Dusseault, M. B., Mraz, D. Z. (1988): Characterization of saltrock creep behavior. In: Proc., 29th U.S. Symp., University of Minnesota, Minneapolis, 179–189.

Hansen, F. D., Mellegard, K. D., Senseny, P. E. (1981): Elasticity and strength of ten natural rock salts. First Conference on the Mechanical Behavior of Salt, Pennsylvania State University, University Park, 71–83.

Kwon, S. (1996): An investigation of the deformation of underground excavations in salt and potash mines. Ph.D. thesis, University of Missouri-Rolla.

Kwon, S., Miller, H. (1995): A new technique for describing the deformation behavior of the rock mass around an underground opening in salt. In: Proc., 35th U.S. Symposium on Rock Mechanics, University of Nevada, Reno, 425–430.

Munson, D. E., et al. (1990): Overtest for simulated defense high-level waste (Room B): In situ data report, SAND 89–2671, Sandia National Laboratories, Albuquerque, New Mexico.

Sakurai, S. (1991): Computational methods in rock mechanics. In: Proc., 7th International Congress on Rock Mechanics, Aachen, Germany, 1563–1570.

Sakurai, S. (1993): Back analysis in rock engineering. Compr. Rock Engng. 4, 543–569.

Senseny, P. E., et al. (1992): Mechanical behavior of rock salt: phenomenology and micromechanisms. Int. J. Rock Mech. Min. Sci. Geomech. Abstr. 29, 363–378.

U.S.DOE (1989): Geotechnical field data and analysis report, DOE/WIPP 89–009.

U.S.DOE (1991): Waste Isolation Pilot Plant supplementary roof support system underground storage area Panel 1, Room 1, DOE/WIPP 91–057.

U.S.DOE (1993): The current bases for roof fall prediction at WIPP and a preliminary prediction for SPDV Room 2. DOE/WIPP 93–033.

U.S.DOE (1994): Investigation of the advantages of removing highly fractured roof beams. DOE/WIPP 94–025.

Verdeman, S. B. (1993): Statistics for engineering problem solving. PWS Publishing Co., Boston.

Wittaker, B. N., Singh, R. N., Sun, G. (1992): Rock fracture mechanics: principles, design, and applications. Wiley, New York.

Authors' address: Prof. John W. Wilson, Department of Mining Engineering, University of Missouri, 226, V.H. McNult Hall, 1870 Miner Circle, Rolla, MO65409-0450 U.S.A.